Fuel, Volume 181, 1 October 2016, Pages 522–530
DOI:10.1016/j.fuel.2016.05.035

Simulation of the calcination of a core-in-shell $CuO/CaCO_3$ particle for Ca-Cu chemical looping

Changlei Qin [a,*], *Vasilije Manovic* [b,*], *Jingyu Ran* [a], *and Bo Feng* [c]

[a] Key Laboratory of Low-grade Energy Utilization Technologies and Systems of Ministry of Education, College of Power Engineering, Chongqing University, Chongqing 400044, China

[b] Combustion and CCS Centre, Cranfield University, Cranfield, Bedfordshire MK43 0AL, United Kingdom

[c] School of Mechanical and Mining Engineering, The University of Queensland, St Lucia, Queensland 4072, Australia

[*] Corresponding author:

Email: c.qin@cqu.edu.cn (Changlei Qin); v.manovic@cranfield.ac.uk (Vasilije Manovic)

ABSTRACT

The internal heat balance through heat generation due to CuO reduction and its consumption by $CaCO_3$ decomposition makes calcination a critical step in a novel Ca-Cu chemical looping process (CaL-CLC). Thus, the calcination behaviour of composite Ca/Cu particles needs to be well understood, especially taking into account that mismatching of heat generation and consumption in the particles can lead to local superheating, agglomeration and loss of activity due to enhanced sintering. In this work, a composite particle model was developed to study the calcination behaviour within a spherical core-in-shell type of particle containing grains of CuO and $CaCO_3$. Simulation results showed that ambient temperature, shell porosity, particle size, and $CaCO_3$ grain size significantly affected the CuO and $CaCO_3$ reaction processes, while the impact of initial particle temperature and CuO grain size can be ignored in the range of parameters considered in the study. By comparison of different types of particles, it was concluded that the core-in-shell pattern was more advantageous if such particles are being applied in CaL-CLC cycles due to better matching in reaction kinetics resulting in more stable and uniform particle temperature distribution during the calcination stage.

Keywords: Ca-Cu chemical looping; CO_2 capture; core-in-shell particle; composite particle model

1. INTRODUCTION

Global warming is becoming a severe problem attracting attention worldwide, due to the increasing atmospheric concentrations of greenhouse gases (mainly CO_2, CH_4 and N_2O). Among these greenhouse gases, carbon dioxide accounts for half of the enhanced greenhouse effect and needs the most urgent treatment [1]. CO_2 capture and sequestration (CCS) has been identified as one of the most significant ways to control CO_2 emissions, and it could contribute 15-55% of the cumulative mitigation of atmospheric CO_2 by 2100 [2].

Calcium looping (CaL), particularly interesting for the cheap sorbents and high CO_2 carrying capacity, is a cost-effective method of capturing CO_2 [3-5]. CaL has been rapidly developing, and the continuous improvement of the process has resulted in its latest derivation, Ca-Cu chemical looping (CaL-CLC) [6, 7]. CaL-CLC could eliminate the energy intensively and costly air-separation unit in the conventional CaL process by introducing a new chemical loop using CuO as the oxygen carrier, which could feed a large amount of heat by its exothermic reduction for the highly endothermic regeneration of CaO-based sorbents. Currently, the research on CaL-CLC is still in its early stage and only limited work has been carried out on its development. Fernández et al. [8-10] reported a detailed conceptual design of Ca-Cu chemical looping to obtain hydrogen and/or electricity from natural gas and a concentrated stream of CO_2 in fixed-bed reactors. Rahman et al. [11] discussed the integration of CaL-CLC with steam gasification of biomass with the carbonator (gasifier), calciner, and air reactor arranged in three sequences. Our team also worked in promoting the development of CaL-CLC, including the report of the inhibition of CaO carbonation by CuO/Cu components [12], the mitigation methods [13], and the assessment of kinetics matching on the calciner level [14].

It was well-known that the arrangement of CuO and $CaCO_3$ in composite particles was an important issue for the effective implementation of the CaL-CLC processes [9, 14]. Taking into account the heat transfer efficiency and potential pressure drop inside the reactor, sorbents were usually prepared in the form of spherical particles, with a combination of Ca-based and Cu-based materials, uniformly arranged

or in a core-in-shell pattern, or as separated particles [9, 15]. Kierzkoska and Müller [16] investigated the synthesis of Ca-based, Cu-functionalised CO_2 composites using a co-precipitation technique. Manovic et al. [17, 18] prepared three types of pellets by granulation of powdered materials using a mechanical pelletiser. The first type of pellet has a homogeneous distribution of CaO and CuO supported by cement, and the other two types were both of the core-in-shell form but with different arrangements of the active (CaO and CuO) and inert (cement) materials. They were shown to be suitable for large-scale utilisation as no significant change in particle size was observed during a 2-h attrition test in a bubbling fluidised bed. In contrast, Ridha et al. [15] reported a lower mechanical strength of core-in-shell particles due to their susceptibility to fragmentation, in comparison to homogeneous particles and mixed CaO-based and CuO-based particles.

It should be noted that the implementation of CaL-CLC largely depends on the effectiveness of internal heat transfer from the reduction of CuO to the decomposition of $CaCO_3$ within a single particle. The synchronism of these two reactions is important and the coupling behaviour needs to be assessed. Work on core-in-shell particles with CuO as core and $CaCO_3$ as shell, which show potential in the CaL-CLC application, has not been previously reported. Aiming to better understand the calcination behaviour of core-in-shell particles during the calcination stage in CaL-CLC, a composite particle model was developed to study the impact of operating conditions and particle parameters on the occurrence of chemical reactions, gas species and heat profiles inside the particle. Furthermore, a comparison between the performance of core-in-shell and uniformly-distributed particles was carried out based on the simulation results.

2. COMPOSITE PARTICLE MODELING

The concept of the changing grain size model (CGSM) proposed by Georgakis et al. [19], has been widely used in the literature [20-24]. In the present work, the model was further developed aiming to understand the calcination behaviour of a core-in-shell particle with CuO and $CaCO_3$ grains distributed in the core and shell, respectively. A CuO/$CaCO_3$ molar ratio of 3.2 was used in the particle simulation

considering the theoretical internal energy balance of chemical reactions. It was assumed that the particle was porous and its radius remained constant during reactions, meaning that shrinkage of the particle caused by sintering was omitted. The particle core also followed this assumption. The size of the material grains changed as a result of the conversion of solid reactant to a product during the reduction of CuO, as shown of Equation 1 (12.4 cm^3/mol of CuO vs. 7.1 cm^3/mol of Cu), and the decomposition of $CaCO_3$, as shown of Equation 2 (36.9 cm^3/mol of $CaCO_3$ vs. 16.9 cm^3/mol of CaO). Physical model of the core-in-shell particle and the change of grains during reactions are shown in Figure 1.

$$CH_{4(g)} + 4CuO_{(s)} = 4Cu_{(s)} + CO_{2(g)} + 2H_2O_{(g)} \quad \Delta H_{r,1173K} = -207.6\,kJ/mol \tag{1}$$

$$CaCO_{3(s)} = CaO_{(s)} + CO_{2(s)} \quad \Delta H_{r,1173K} = 165.6\,kJ/mol \tag{2}$$

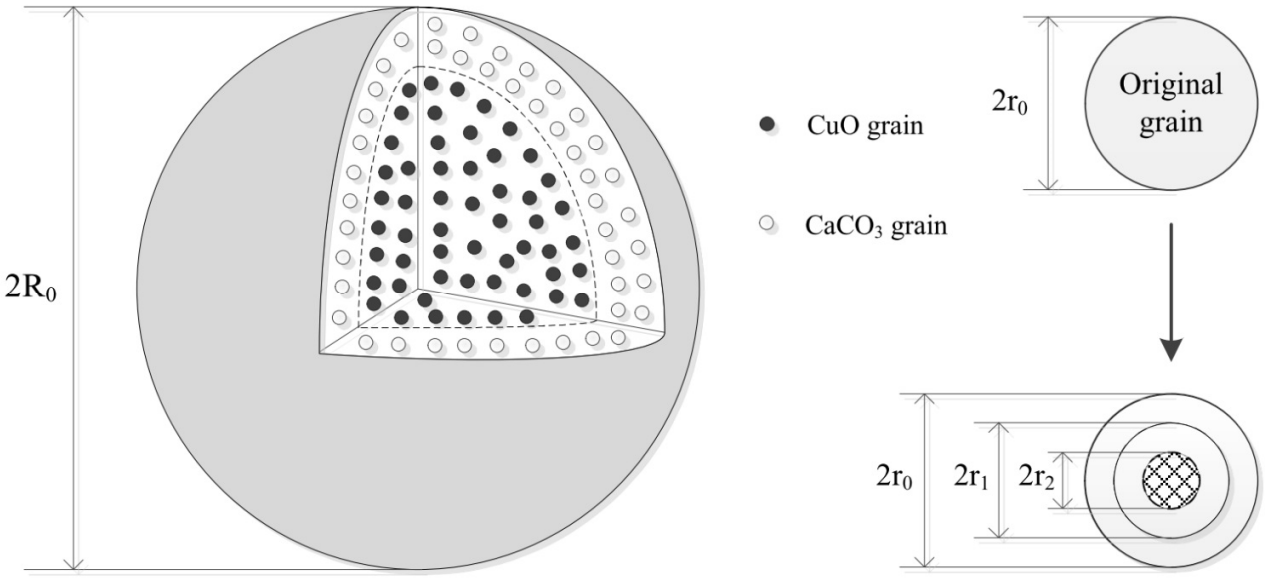

Figure 1. Schematic of the core-in-shell $CuO/CaCO_3$ particle and the variation of a grain during calcination.

For the specific core-in-shell particle, core radius is a function of the initial core and shell porosity and the radius of the whole particle. Core radius is calculated as follows:

$$\frac{R_{0,core}^3}{R_0^3}=\frac{3.2V_{m,CuO}\left(1-\varepsilon_{0,shell}\right)}{3.2V_{m,CuO}\left(1-\varepsilon_{0,shell}\right)+V_{m,CaCO_3}\left(1-\varepsilon_{0,core}\right)} \tag{3}$$

The mass balance for diffusion and reaction of gas 'i' inside the particle is given as follows:

$$\frac{\partial C_i}{\partial t}=\frac{1}{R^2}\frac{\partial}{\partial R}\left(D_{e,i}R^2\frac{\partial C_i}{\partial R}\right)+r_i \tag{4}$$

The initial and boundary conditions required for solving the equation coupling external mass transfer are as follows,

$$C_i(R,t)=C_{i,0},\quad t=0 \tag{5}$$

$$\left.\frac{\partial C_i}{\partial R}\right|_{R=0}=0,\quad t\geq 0 \tag{6}$$

$$-D_{e,i}\left.\frac{\partial C_i}{\partial R}\right|_{R=R_0}=k_{g,i}\left(C_{s,i}-C_{b,i}\right),\quad t\geq 0 \tag{7}$$

The external mass transfer coefficient of $k_{g,i}$ was calculated using the Sherwood number given by [25],

$$Sh=\frac{2k_{g,i}R_0}{D_{m,i}}=2+0.6\,Re^{1/2}\,Sc^{1/3} \tag{8}$$

The reaction rate of gas 'i' produced or consumed per unit of particle volume was proportional to the chemical reaction rate constant k, and the following expressions with kinetic parameters for the reduction of CuO with CH_4 and the decomposition of $CaCO_3$ [20, 26] were chosen for this work because of their close fitting with the experimental data.

$$r_{CuO}=-k_{red}S_{0,CuO}\left(\frac{r_{2,CuO}}{r_{0,CuO}}\right)^2C_{CH_4}^n \tag{9}$$

$$r_{CaCO_3}=-k_{dec}S_{0,CaCO_3}\left(\frac{r_{2,CaCO_3}}{r_{0,CaCO_3}}\right)^2\left(1-\frac{C_{CO_2}}{C_{eq,CO_2}}\right) \tag{10}$$

$$C_{eq,CO_2}=\frac{1.462\times10^{11}}{T}exp\left(-\frac{19130}{T}\right) \tag{11}$$

$$k_{red} = 0.5 exp\left(-\frac{40600}{gasR \cdot T} \right) \tag{12}$$

$$k_{dec} = 254 exp\left(-\frac{131000}{gasR \cdot T} \right) \tag{13}$$

The initial specific surface of solid reactant ‘j’ was calculated as:

$$S_{0,j} = \frac{3(1-\varepsilon_0)}{r_{0,j}} f_{v,j} \tag{14}$$

The radius variation of unreacted solid reactant was determined from the chemical reaction rate taking place at the reaction interface with the equations:

$$\frac{dr_{2,CuO}}{dt} = -k_{red} V_{m,CuO} C_{CH_4}^n \tag{15}$$

$$\frac{dr_{2,CaCO_3}}{dt} = -k_{dec} V_{m,CaCO_3} \left(1 - \frac{C_{CO_2}}{C_{eq,CO_2}} \right) \tag{16}$$

The changing grain size of $r_{1,j}$ was calculated as:

$$r_{1,j}^3 = Z_j r_0^3 + (1 - Z_j) r_{2,j}^3 \tag{17}$$

where Z_j was defined as:

$$Z_j = \frac{V_{m,P}}{V_{m,R}} \tag{18}$$

The effective diffusivity of gas ‘i’ was calculated as a function of particle porosity as:

$$D_{e,i} = \left(D_{m,i}^{-1} + D_{K,i}^{-1} \right)^{-1} \varepsilon^2 \tag{19}$$

Particle porosity varies as a function of the initial porosity during reactions, and was calculated as:

$$\varepsilon = \varepsilon_0 - \sum \left[f_{v,j,0} (Z_j - 1)(1 - \varepsilon_0) X_j(R,T) \right] \tag{20}$$

The molecular diffusivity of gas ‘i’ in the gas mixture was calculated by the Wilke equation:

$$D_{m,i} = \frac{1-y_i}{\sum_{l=1,l\neq i}^{n} \frac{y_l}{D_{m(i,l)}}} \tag{21}$$

where $D_{m(i,l)}$ expresses the molecular diffusivity of gas 'i' in gas 'l', and it was calculated using the following equation [27]:

$$D_{m(i,l)} = \frac{3.2\times10^{-4} T^{1.75}\left(M_i^{-1}+M_l^{-1}\right)^{0.5}}{P\left[\left(\sum v\right)_i^{1/3}+\left(\sum v\right)_l^{1/3}\right]^2} \tag{22}$$

The Knudsen diffusivity was calculated from:

$$D_{K,i} = \frac{6.135\varepsilon}{S_e}\sqrt{\frac{T}{M_i}} \tag{23}$$

The specific surface area of solid was calculated from the surface area of reactants:

$$S_e = \sum_{j=1}^{n}\left[S_{0,j}\left(\frac{r_{1,j}}{r_{0,j}}\right)^2\right] \tag{24}$$

Local conversion inside the particle changes with time and location, and it was calculated as:

$$X_j\left(R,t\right) = 1-\left(\frac{r_{2,j}}{r_{0,j}}\right)^3 \tag{25}$$

The mean conversion of CuO and $CaCO_3$ changing with time in the whole particle was calculated by integration of local conversions:

$$X_{CuO}\left(t\right) = \frac{\int_0^{R_{0,CuO}} 4\pi R^2 X_j\left(R,t\right) dR}{\frac{4}{3}\pi R_{0,CuO}^3} \tag{26}$$

$$X_{CaCO_3}\left(t\right) = \frac{\int_{R_{0,CuO}}^{R_0} 4\pi R^2 X_j\left(R,t\right) dR}{\frac{4}{3}\pi\left(R_0^3 - R_{0,CuO}^3\right)} \tag{27}$$

For a spherical particle, the unsteady state heat transfer equation can be written as:

$$\overline{\rho c_p}\frac{\partial T}{\partial t}=\frac{1}{R^2}\frac{\partial}{\partial R}\left(\lambda_{ef}R^2\frac{\partial T}{\partial R}\right)+r_{CaCO_3}\Delta H_{dec}+r_{CuO}\Delta H_{red} \tag{28}$$

with the initial and boundary conditions being given as follows:

$$T=T_0,\quad t=0 \tag{29}$$

$$\left.\frac{\partial T}{\partial R}\right|_{R=0}=0,\quad t\geq 0 \tag{30}$$

$$\lambda_{ef}\left.\frac{\partial T}{\partial R}\right|_{R=R_0}=h_c\left(T_b-T_s\right)+e\sigma\left(T_b^4-T_s^4\right),\quad t\geq 0 \tag{31}$$

The heat convection coefficient in Equation (31) was estimated using the Nusselt number with the correlation of Ranz and Marshall [28, 29] :

$$h_c=\frac{Nu\lambda_g}{2R_0} \tag{32}$$

$$Nu=2.0+0.6\,Re^{0.5}\,Pr^{0.33} \tag{33}$$

The effective thermal conductivity of the particle depends on solid and gas thermal conductivities as functions of porosity, and is calculated as follows:

$$\lambda_{ef}=\frac{1}{3}\left[\varepsilon\lambda_g+\left(1-\varepsilon\right)\lambda_s\right]+\frac{2}{3}\left[\frac{\varepsilon}{\lambda_g}+\frac{1-\varepsilon}{\lambda_s}\right]^{-1} \tag{34}$$

The thermal conductivity of the solid in a particle was calculated as a function of the volume fraction of solid components in the particle, given as:

$$\lambda_s=\frac{1}{\sum\frac{f_{v,j}}{\lambda_{s,j}}} \tag{35}$$

The thermal conductivity of the gas mixture in a particle was calculated using the following equation:

$$\lambda_g=\sum_{i=1}^{n}\frac{y_i\lambda_{g,i}}{\sum_{l=1}^{n}y_lA_{il}} \tag{36}$$

with

$$A_{il} = \frac{\left[1+\left(\frac{\mu_i}{\mu_l}\right)^{0.5}\left(\frac{M_i}{M_l}\right)^{0.25}\right]^2}{8^{0.5}\left[1+\left(\frac{M_i}{M_l}\right)\right]^{0.5}} \quad (37)$$

The effective heat capacity was obtained by the following relation:

$$\overline{\rho c_p} = (1-\varepsilon)\rho_s c_{p,s} + \varepsilon\rho_g c_{p,g} \quad (38)$$

These equations were solved numerically on MATLAB v 7.9 by a finite volume method with a fully implicit formulation and a time step of 10^{-4} s, and a convergence with a tolerance less than 10^{-6} was chosen during the calculations in the work.

To verify the model, overall conversions of CuO and $CaCO_3$ were obtained by calculation using the developed model and from experiments in a thermogravimetric analyser. Considering the difficulty in distinguishing the mass loss caused by CuO reduction and $CaCO_3$ decomposition, the experiments were carried out by testing the two reactions separately under isothermal conditions, and pure calcium carbonate and CuO/alumina materials were utilised. During the testing, the total gas flow rate was maintained at 100 mL/min, and conversions were calculated with the assumption that the mass loss was only caused by the reactions studied. Figure 2 shows the comparison of the simulation and experimental results, and it can be seen that the model developed properly predicts the rate of CuO reduction with CH_4 and the decomposition of $CaCO_3$.

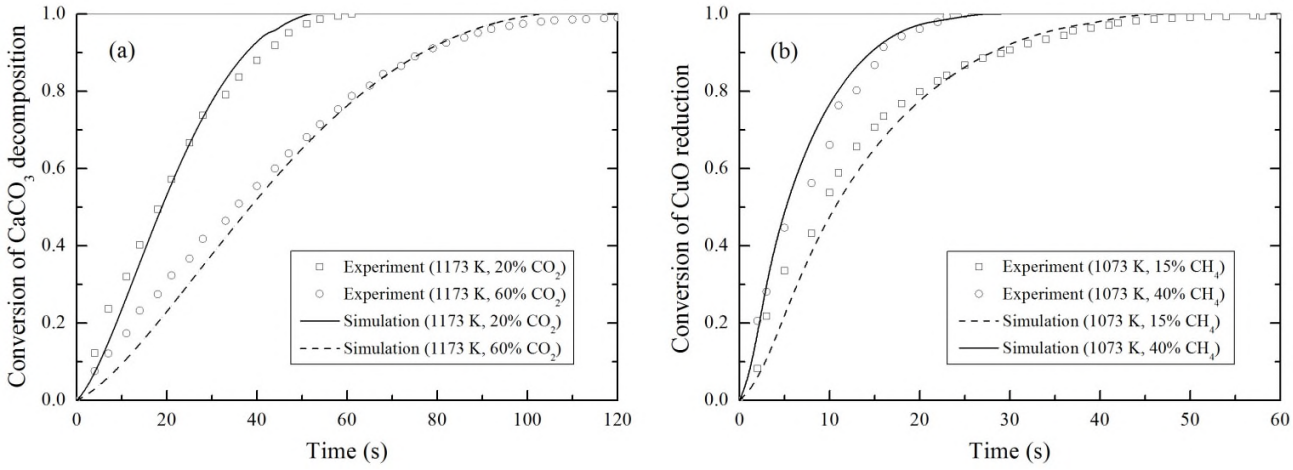

Figure 2. Comparison of simulation and experimental results of the conversion rate of (a) $CaCO_3$ decomposition and (b) CuO reduction with CH_4.

3. RESULTS AND DISCUSSION

To have a comprehensive view of the change in key variables with time, concentration profiles of CH_4 and CO_2, local temperature, porosity, local CuO and $CaCO_3$ conversion, and grain size of CuO and $CaCO_3$ inside the spherical particle were displayed in a three-dimensional graph, as shown in Figure S1 in the supporting information. It was obtained by simulating a particle characterised with a porosity of 0.3 in both the core and shell, which were composed of CuO grains of 500 nm in radius and $CaCO_3$ grains of 200 nm in radius, respectively. CuO and $CaCO_3$ parameters used in the work were determined according to the experimental data and calculation formulas presented in the literature [20, 26, 30-32]. The simulation was carried out for an ambient temperature of 1173 K and 0.2 bar of CH_4 (balance CO_2) at atmospheric pressure with an initial particle temperature of 1173 K. Additionally, radial profiles of variables at specific times under the same conditions as above are summarised in Figure 3.

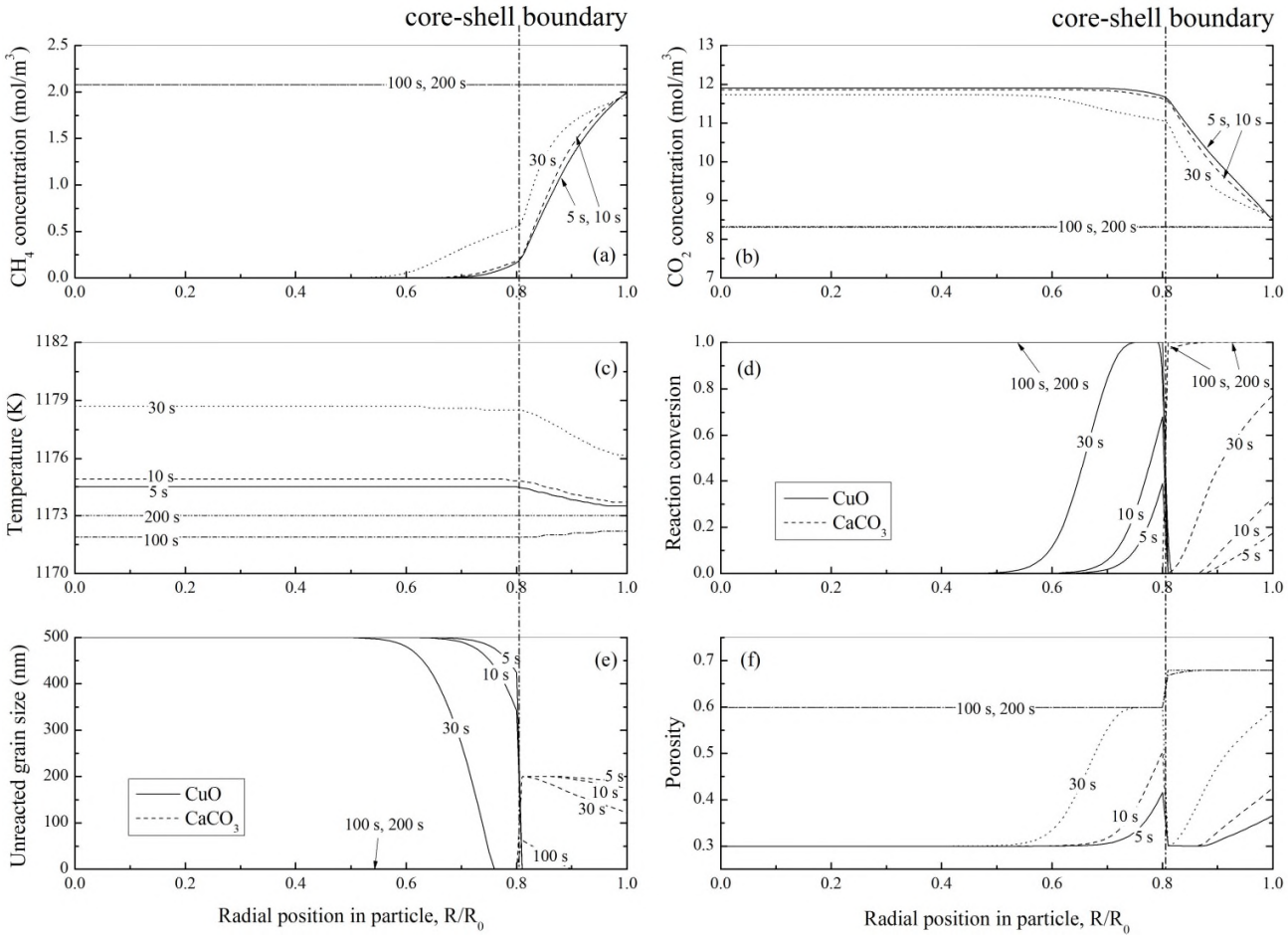

Figure 3. Variation of radial distribution of some parameters within the particle with time (P_{CH_4} = 0.2 bar, P_{CO_2} = 0.8 bar; T_b = 1173 K, T_0 = 1173 K; $\varepsilon_{0,CuO} = \varepsilon_{0,CaCO_3} = 0.3$, R_0 = 1 mm, $r_{0,CuO}$ = 500 nm, $r_{0,CaCO_3}$ = 200 nm).

A sharp initial decrease in CH_4 concentration from the particle surface to its centre can be seen in Figure 3. At 5 s, CH_4 concentration on the particle surface was 2 mol/m^3 and it declined to around 0.2 mol/m^3 on the core-shell boundary. Moreover, no CH_4 was observed in the area of $R/R_0<0.62$. This type of CH_4 distribution within the particle is a consequence of diffusion resistance in the $CaCO_3$ shell owing to the low shell porosity and its high effective specific surface area. Thereby, the reduction of CuO with CH_4 was very slow in the particle core area. In contrast, CO_2 concentration was highest and almost constant in the particle core, and it decreased from the core-shell boundary to the particle surface, which

was attributed to the combined effect of CO_2 generation due to $CaCO_3$ decomposition and CuO reduction, and the varying local CO_2 diffusivity in the particle.

Figure 3(c) shows that the temperature profile inside the particle was relatively flat over the studied duration. It was constant at just above 1174 K in the core area and the value was a little lower on the particle surface after 5 s, which was almost the same after 10 s. The profile of a slightly higher temperature can be observed during the following 48 s without the appearance of a significant temperature difference, implying that heat transfer in the particle and subsequent consumption due to $CaCO_3$ decomposition were well matched with CuO reduction. Then, particle temperature started to decline slowly and reached a minimum value at around 68 s with the core temperature being slightly lower than that in the shell, indicating the completion of CuO reduction and heat transfer from the surroundings for the decomposition of $CaCO_3$.

3.1. Effect of Ambient Temperature

The reduction of CuO and decomposition of $CaCO_3$ are the two major reactions in the calcination process of Ca-Cu chemical looping, and their kinetics are mainly determined by operating temperature according to the Arrhenius law. Therefore, the influence of ambient temperature on the conversions was investigated and is presented in Figure 4, for a particle of 1 mm in radius, with an identical initial porosity of 0.3 in both the core (initial CuO grain radius of 500 nm) and the shell (initial $CaCO_3$ grain radius of 200 nm), and an initial particle temperature of 1173 K.

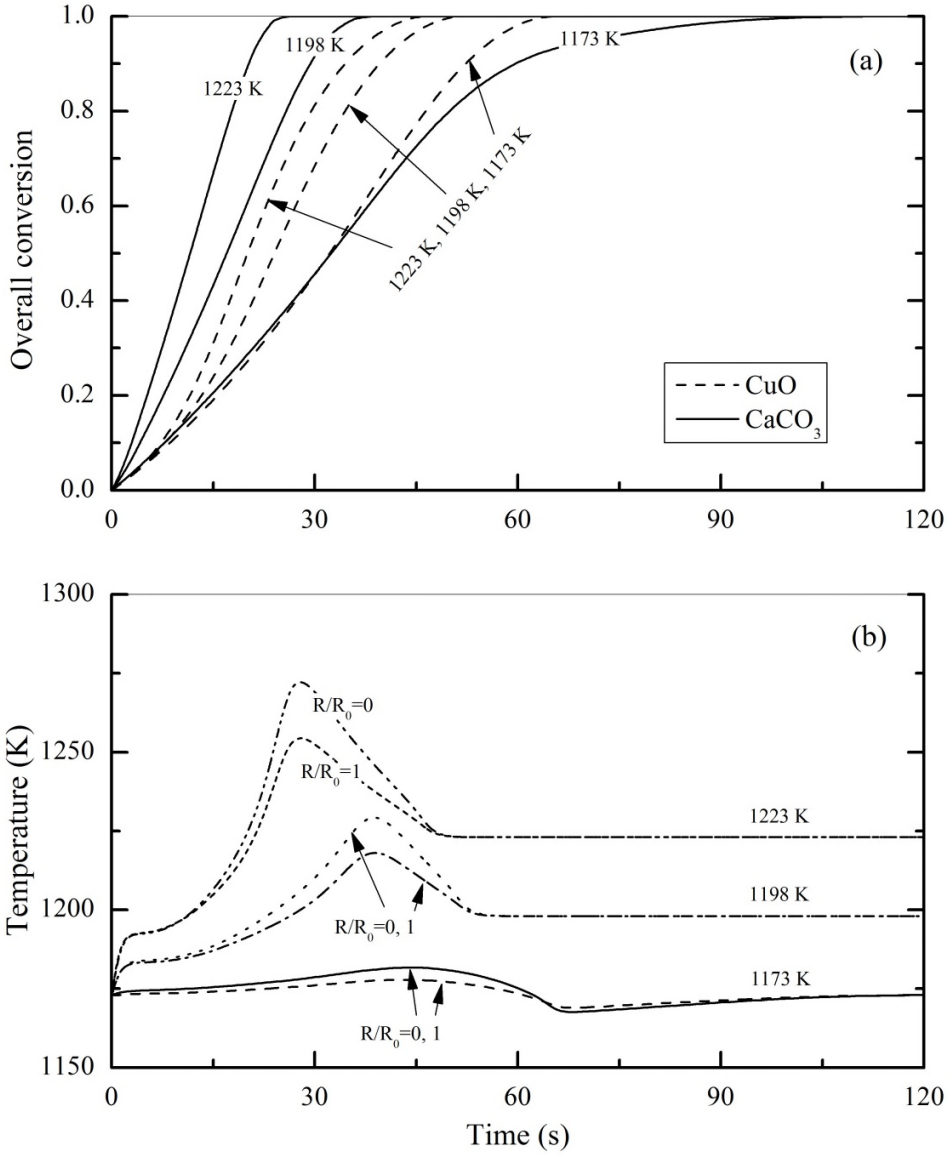

Figure 4. Profiles of temperatures and overall conversions inside the particle under different ambient temperatures (P_{CH_4} = 0.2 bar, P_{CO_2} = 0.8 bar; T_0 = 1173 K; $\varepsilon_{0,CuO} = \varepsilon_{0,CaCO_3}$ = 0.3, R_0 = 1 mm, $r_{0,CuO}$ = 500 nm, $r_{0,CaCO_3}$ = 200 nm).

It can be seen in Figure 4(a) that the overall conversion of CuO was very close to that of $CaCO_3$ decomposition at an ambient temperature of 1173 K, although the latter proceeded slightly faster during the first 30 s. Subsequently, the reduction of CuO gradually became slightly faster. The good coupling of the two reactions, i.e., the almost simultaneous occurrence of CuO reduction and $CaCO_3$

decomposition, can be a benefit for keeping the variation of particle temperature in a narrow range and avoiding the appearance of superheating that can lead to sintering and agglomeration of materials, and consequent loss of the activity and even operating life of the regenerator. Increasing the ambient temperature to 1198 K, the CuO reduction rate was observed to increase more slowly than the rate of $CaCO_3$ decomposition. The reason for this was that while the former reaction was limited by the slow feeding rate of CH_4, the latter could still utilise the heat from the high-temperature surroundings. After $CaCO_3$ decomposition reached completion, a large amount of energy was released from the exothermic reduction of the remaining CuO to heat the particle (the sharp temperature increase in Figure 4(b)). This phenomenon became more apparent when ambient temperature was further increased to 1223 K. Thus, 1173 K was the optimal ambient temperature for the regeneration of sorbents under the conditions studied.

3.2. Effect of Initial Particle Temperature

The initial temperature difference between sorbent particles and the surroundings requires a certain time interval for the particles to reach the designated operating conditions. Thus, the effect of initial particle temperature on conversion and temperature profiles was studied, ranging from 923 K to 1173 K, while keeping the other variables constant. It can be seen from Figure 5 that the induction time for the occurrence of $CaCO_3$ decomposition became longer as decreasing initial particle temperature further deviated from the ambient value, which agreed well with the work of Yin et al. [23] Though both CuO reduction and $CaCO_3$ decomposition became slower, the decline in the reaction rate of the latter was more pronounced. In other words, the mismatching of reaction kinetics and heat transfer in the regenerator could become more prominent by increasing the difference between initial particle temperature and that of the surroundings.

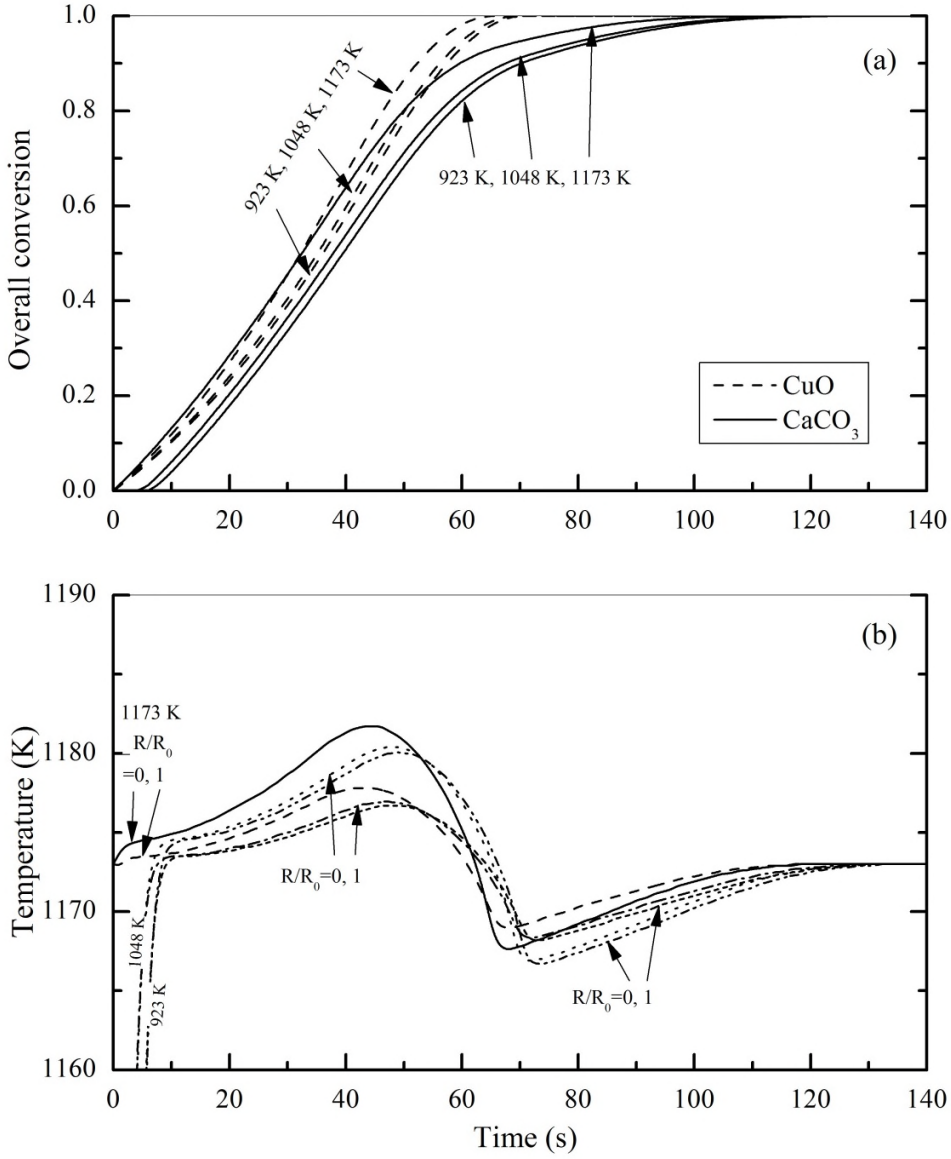

Figure 5. Profiles of temperatures and overall conversions inside the particle while varying initial particle temperature from 923 K to 1173 K (P_{CH_4} = 0.2 bar, P_{CO_2} = 0.8 bar; T_b = 1173 K; $\varepsilon_{0,CuO} = \varepsilon_{0,CaCO_3}$ = 0.3, R_0 = 1 mm, $r_{0,CuO}$ = 500 nm, $r_{0,CaCO_3}$ = 200 nm).

3.3. Effect of Particle Porosity

It is well known that porosity largely determines physical and chemical properties of a particle, such as its crushing strength, attrition rate, inner gas diffusion, and reactivity [33], and the effect can be more significant for core-in-shell particles because the feeding of CH_4 from the surroundings to the core area

is restrained by the matrix of $CaCO_3$ grains in the shell. To understand the potential impact, the porosities of CuO in the core and $CaCO_3$ in the shell were varied, respectively, from 0.1 to 0.5 and the generated conversion profiles are presented in Figure 6. It can be seen that the overall conversion of CuO rose with the increase of initial core porosity due to a lower resistance to the diffusion of CH_4 into the core region. As CuO reduction was the main heat source for $CaCO_3$ calcination, the process of $CaCO_3$ decomposition changed accordingly and its variation was easily understood to be slightly smaller than that of CuO. It was interesting to note from Figure 6(a) that coupling of the reactions of CuO and $CaCO_3$ changed only marginally with varying CuO porosity under the conditions studied.

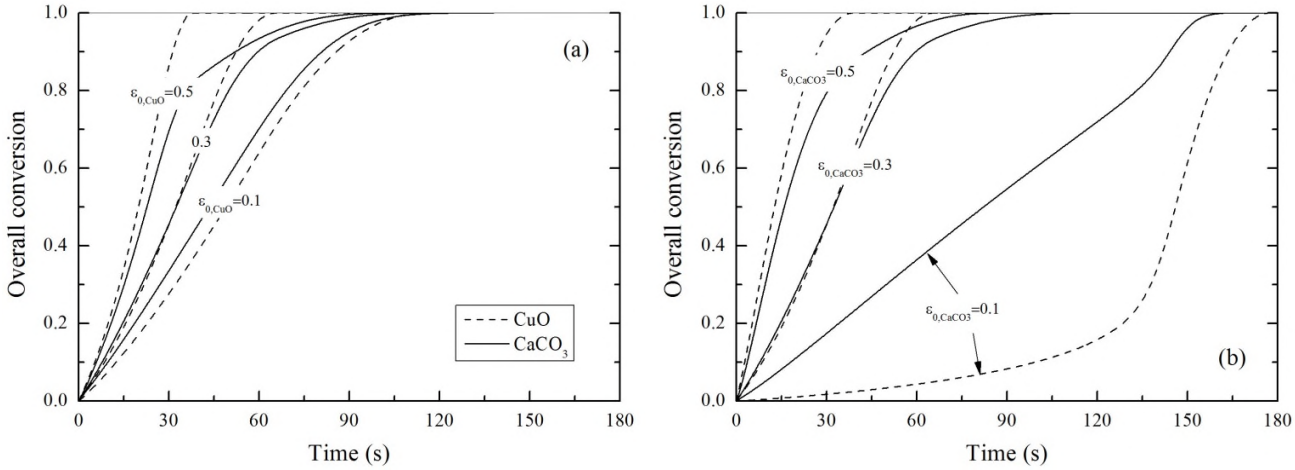

Figure 6. Profiles of overall conversions inside the particle with varying initial porosity of (a) particle core, and (b) particle shell (P_{CH_4} = 0.2 bar, P_{CO_2} = 0.8 bar; T_b = 1173 K, T_0 = 1173 K; R_0 = 1 mm, $r_{0,CuO}$ = 500 nm, $r_{0,CaCO_3}$ = 200 nm).

Figure 6(b) shows the profile of overall conversions as a function of initial shell porosity. It was known that the existence of a shell containing $CaCO_3$ grains was the main barrier for the penetration of CH_4 from the ambient to the particle core. The decrease of initial $CaCO_3$ porosity caused a reduction in its specific surface area, which together led to a sharp fall-off of effective diffusivity of CH_4 in the shell. As a result, overall conversion of CuO was observed to decline quickly. With regard to $CaCO_3$

decomposition, it was also largely inhibited owing to the lack of heat supply from CuO reduction. This condition remained unchanged until much of the $CaCO_3$ was converted, at which point the rate of CuO reduction with CH_4 increased quickly. When increasing the initial porosity of $CaCO_3$ to 0.5, its inhibition on CH_4 diffusion was weakened. Thus CuO reduction became much faster, and the calcination of $CaCO_3$ was enhanced. However, process matching of the two reactions was slightly poorer at a shell porosity of 0.5 than that with a value of 0.3.

3.4. Effect of Particle Size

Particle size usually affects reaction rates and external mass and heat transfer, which has been observed in the single reduction of CuO and $CaCO_3$ decomposition [20, 33]. Here, we investigated the core-in-shell CuO/$CaCO_3$ composite by varying particle radius from 0.5 mm to 1.5 mm, and summarised the results in Figure 7. It was apparent that the conversion of both CuO and $CaCO_3$ decreased with increasing particle radius. For the particle with a radius of 1 mm, CuO and $CaCO_3$ achieved full conversion in 66 s and 117 s, respectively, which were extended to 135 s and 146 s at a particle radius of 1.5 mm. The heat released from CuO reduction could still be used in calcining $CaCO_3$, but the efficiency varied according to the reaction process. As can be seen for the particle with a radius of 0.5 mm, the rate of CuO reduction was much faster than $CaCO_3$ decomposition, thus a large amount of energy was released over a short time and the whole particle was heated up. After all CuO was consumed, some of the $CaCO_3$ remained unreacted and its further reaction would depend on the heat transferred from the surroundings, which resulted in a lower particle temperature than that of the ambient. For the 1.5-mm-radius particle, the reaction process of CuO was slightly behind $CaCO_3$ decomposition for most of the time; therefore, the particle temperature was below the ambient temperature. It was clear that once the reaction rate of CuO exceeded that of $CaCO_3$, the heat released was sufficient to support $CaCO_3$ decomposition and particle temperature would rise to higher than that of the surroundings, as shown in Figure 7(b).

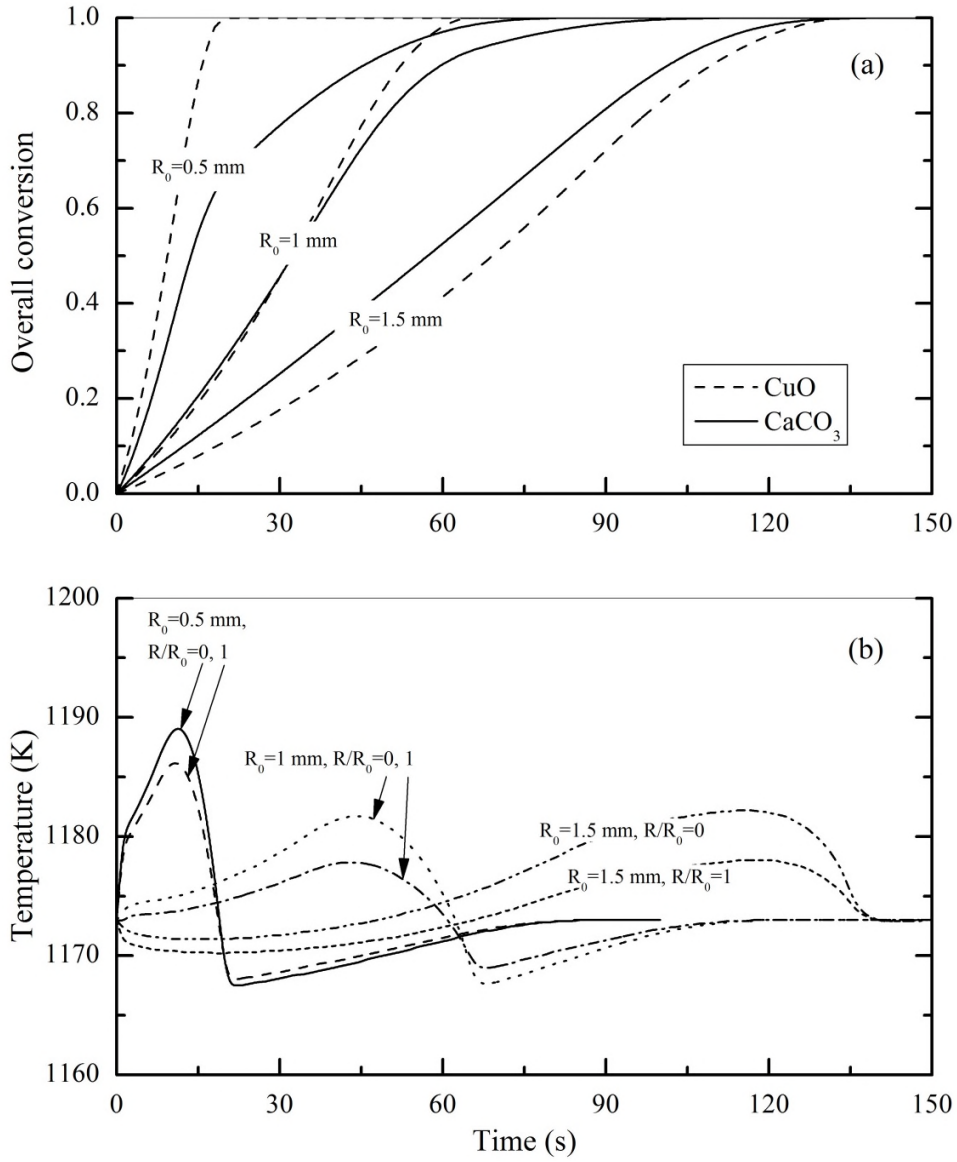

Figure 7. Profiles of overall conversions and temperatures inside the particle with varying particle radius (P_{CH_4} = 0.2 bar, P_{CO_2} = 0.8 bar; T_b = 1173 K; T_0 = 1173 K; $\varepsilon_{0,CuO} = \varepsilon_{0,CaCO_3} = 0.3$, $r_{0,CuO}$ = 500 nm, $r_{0,CaCO_3}$ = 200 nm).

3.5. Effect of Grain Size

The potential effect of grain size variation on calcination behaviour was investigated by changing

grain radius of CuO and $CaCO_3$ in the range of 200 nm to 800 nm, and the results are summarised in Figure 8. It can be seen that overall conversion profiles of CuO were almost identical, regardless of the variation of CuO grain size. The distribution of $CaCO_3$ conversion with time was also maintained. These observations mean that CuO grain size in the range investigated has almost no effect on the simultaneous reaction behaviour of CuO and $CaCO_3$ during regeneration. The reason for this is that the reduction of CuO is kinetically fast under the conditions studied, and only the supply of CH_4 from the surroundings via the shell could be a limitation. However, the diffusion of CH_4 was unaffected when varying grain size of CuO in the core area. As a result, the decomposition process of $CaCO_3$ remained unchanged as well. By contrast, the rate of CuO reduction became faster with increased initial $CaCO_3$ grain radius, which slightly accelerated $CaCO_3$ decomposition initially, as shown in Figure 8(b). As CuO reduction finished, the decomposition rate of $CaCO_3$ in the case of a larger initial grain size decreased more quickly and the time required to reach 100% conversion was prolonged.

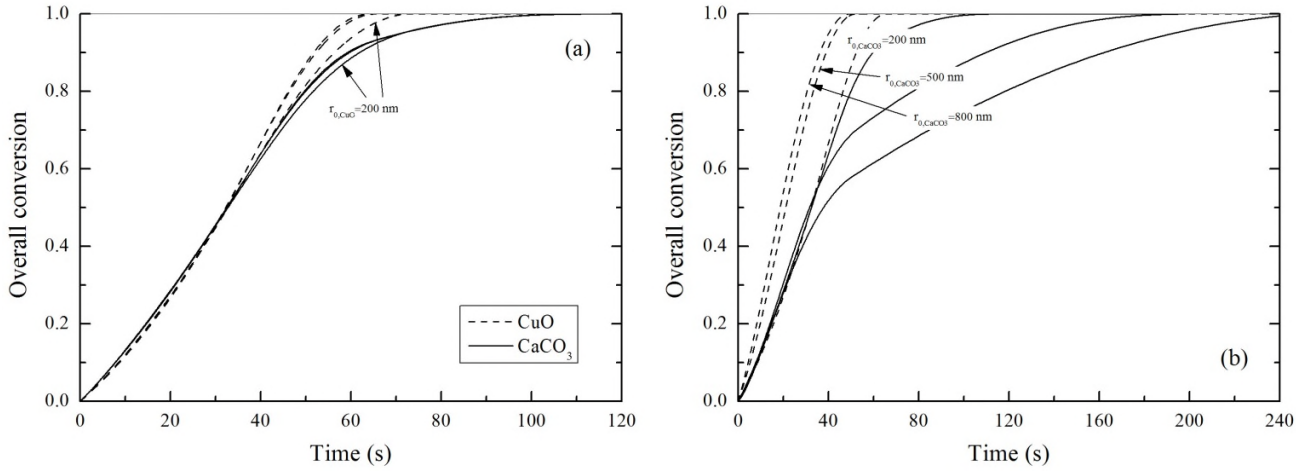

Figure 8. Profiles of overall conversions inside the particle with varying initial grain radius of (a) CuO, and (b) $CaCO_3$ (P_{CH_4} = 0.2 bar, P_{CO_2} = 0.8 bar; T_b = 1173 K; T_0 = 1173 K; $\varepsilon_{0,CuO} = \varepsilon_{0,CaCO_3} = 0.3$, R_0 = 1 mm).

3.6. Comparison of Uniformly-distributed and Core-in-shell Particles

Uniform-distribution and core-in-shell patterns are the two most interesting arrangements for CuO and $CaCO_3$ grains in a composite particle that can potentially be used in the CaL-CLC system due to good matching in heat release and the subsequent utilisation. In our previous work [34], the time to reach full conversion of CuO and $CaCO_3$ was calculated to be 35 s and 137 s, respectively, when a particle of 1 mm in radius and 0.3 in porosity with a uniform distribution of CuO and $CaCO_3$ grains (grain size of 500 nm vs. 200 nm) was initialised at 1173 K under 0.2 bar of CH_4. Under the same conditions, the time for reaction completion varied between 66 s and 117 s for the core-in-shell particle. Additional simulation showed that including or neglecting heat radiation between the particle and its surroundings in equation (31) makes no difference for the conditions compared. The time extension for CuO to reach full reduction was clearly attributable to the resistance of the $CaCO_3$ shell to CH_4 diffusion as analysed above. However, its inhibition of CuO reduction could accelerate the occurrence of $CaCO_3$ decomposition and resulted in a more synchronised calcination/reduction, i.e., a better matching of heat release and utilisation. This coupling can be pursued in CaL-CLC system design, as it eliminates the requirement of an external heat source for regenerating $CaCO_3$, which is one inherent advantage of CaL-CLC compared to the conventional calcium looping for CO_2 capture. Furthermore, good matching of CuO reduction and $CaCO_3$ decomposition rates could help to avoid large particle temperature fluctuations with time. This conclusion can be easily observed from the temperature variation range of 55 K for the uniformly-distributed particle and only around 10 K for the core-in-shell type, which is an advantage in preventing superheating and stabilising operation of the regenerator. Therefore, the core-in-shell arrangement was more suitable for application in the calcination stage of CaL-CLC if taking reaction kinetics and heat transfer within particles into consideration.

4. CONCLUSIONS

To well understand the behaviour of reaction coupling (CuO reduction with CH_4 and the

decomposition of $CaCO_3$) and heat transfer in the calcination stage of the novel Ca-Cu chemical looping process, a mathematical model of the composite particle was developed to investigate the core-in-shell arrangement within the framework of the key particle parameters and operating conditions. Simulation results showed that ambient temperature, porosity of the shell, particle size, and $CaCO_3$ grain size significantly affected the reaction process of CuO and $CaCO_3$. A lower ambient temperature, in the range of 1173-1223 K, was observed to be beneficial for coupling of the reactions, while an increase of ambient temperature resulted in faster decomposition of $CaCO_3$ when compared to that of reduction of CuO. Though the coupling behaviour of the two reactions was similar with the change of core porosity from 0.1 to 0.5, a significant decline of the reduction rate of CuO was observed when decreasing the shell porosity from 0.3 to 0.1 as a result of the high resistance of CH_4 diffusion in the shell area. It was also found that the optimal radius of the core-in-shell particle should be around 1 mm or a little larger with a small $CaCO_3$ grain (200 nm) under the conditions studied in this work. In contrast, the effect of CuO grain size and the initial particle temperature can be neglected.

Compared to particles with a uniform distribution of CuO and $CaCO_3$ grains, the core-in-shell arrangement was determined to be beneficial for coupling the CuO reduction with CH_4 and decomposition of $CaCO_3$, with the particle temperature fluctuating only in a narrow range. The model developed can be a useful tool for quantifying trade-offs between the key design and operational parameters of the calcination process in CaL-CLC.

NOTATION

C_{CH_4}	CH_4 concentration within the particle, mol/m^3
C_{CO_2}	CO_2 concentration within the particle, mol/m^3
C_{eq,CO_2}	equilibrium CO_2 concentration, mol/m^3
C_i	concentration of gas ‘i’, mol/m^3

$C_{i,0}$	initial concentration of gas ‘i’ within the particle, mol/m^3
$C_{b,i}$	concentration of gas ‘i’ in the reactor, mol/m^3
$C_{s,i}$	concentration of gas ‘i’ on particle surface, mol/m^3
$c_{p,g}$	specific heat of gas mixture, J/(kg·K)
$c_{p,s}$	specific heat of solid within particle, J/(kg·K)
$D_{e,i}$	effective diffusivity of gas ‘i’, m^2/s
$D_{K,i}$	Knudsen diffusion coefficient of gas ‘i’, m^2/s
$D_{m,i}$	molecular diffusion coefficient of gas ‘i’, m^2/s
e	emissivity
$f_{v,j}$	volume fraction of solid ‘j’ within the particle
$f_{v,j,0}$	initial volume fraction of solid ‘j’ within the particle
gasR	gas constant, J/(mol·K)
h_c	external heat transfer coefficient, W/(m^2·K)
$k_{g,i}$	external mass transfer coefficient of gas ‘i’, m/s
k_{red}	reaction rate constant of CuO reduction, m$^{1.3875}$/(mol$^{0.4625}$·s)
k_{dec}	reaction rate constant of $CaCO_3$ decomposition, m^3/(mol·s)
M_i	molecular weight of gas ‘i’, kg/mol
M_l	molecular weight of gas ‘l’, kg/mol
Nu	Nusselt number
n	reaction order of the reduction of CuO with CH_4
P	total pressure, Pa
Pr	Prandtl number

r_i	production rate of gas ‘i’, mol/(m^3·s)
r_{CuO}	rate of CuO reduction, mol/(m^3·s)
r_{CaCO_3}	rate of $CaCO_3$ decomposition, mol/(m^3·s)
$r_{0,j}$	initial grain radius of solid ‘j’, m
$r_{1,j}$	grain radius of solid ‘j’ when reaction proceed, m
$r_{2,j}$	grain radius of unreacted solid ‘j’, m
$r_{0,CuO}$	initial grain radius of CuO, m
$r_{2,CuO}$	grain radius of unreacted CuO, m
$r_{0,CaCO_3}$	initial grain radius of $CaCO_3$, m
$r_{2,CaCO_3}$	grain radius of unreacted $CaCO_3$, m
R	radial coordinate, m
R_0	initial radius of the particle, m
Re	Reynolds number
$S_{0,CuO}$	initial specific surface area of CuO, m^2/m^3
$S_{0,CaCO_3}$	initial specific surface area of $CaCO_3$, m^2/m^3
$S_{0,j}$	initial specific surface area of solid reactant ‘j’, m^2/m^3
S_e	specific surface area of the solid, m^2/m^3
Sc	Schmidt number
Sh	Sherwood number
t	time, s
T	temperature, K
T_0	initial particle temperature, K

T_b temperature in the reactor, K

T_s temperature of the particle surface, K

$V_{m,CuO}$ molar volume of CuO, m^3/mol

$V_{m,CaCO_3}$ molar volume of $CaCO_3$, m^3/mol

$V_{m,P}$ molar volume of solid product, m^3/mol

$V_{m,R}$ molar volume of solid reactant, m^3/mol

X_j conversion of solid reactant ‘j’

y_i molar fraction of gas ‘i’

Z_j volume ratio for solid product to reactant

Greek symbols

ε_0 initial particle porosity

ε particle porosity

λ_g thermal conductivity of the gas mixture, W/(m·K)

λ_{ef} effective thermal conductivity within the particle, W/(m·K)

λ_s thermal conductivity of the solid within the particle, W/(m·K)

$\lambda_{s,j}$ thermal conductivity of solid ‘j’, W/(m·K)

ΔH_{red} heat of CuO reduction, J/mol

ΔH_{dec} heat of $CaCO_3$ decomposition, J/mol

μ_i dynamic viscosity of gas ‘i’, kg/(m·s)

μ_l dynamic viscosity of gas ‘l’, kg/(m·s)

ρ_g density of gas mixture, kg/m^3

ρ_s density of solid within the particle, kg/m^3

$\left(\sum v\right)_i$ diffusion volume for molecule ‘i’

σ Stefan-Boltzman coefficient, W/(m^2·K^4)

ACKNOWLEDGEMENT

The authors are grateful to the financial supports from China Postdoctoral Science Foundation (No. 2015M572448), Chongqing Postdoctoral Funding Project (No. Xm2015002), the Fundamental Research Funds for the Central Universities (No. 106112015CDJXY140005), Key Laboratory of Low-grade Energy Utilization Technologies and Systems of Ministry of Education (No. LLEUTS-201411, LLEUTS-2016004), and the Scientific Research Foundation for the Returned Overseas Chinese Scholars, State Education Ministry.

REFERENCES

[1] IPCC. IPCC Fourth Assessment Report: Climate Change 2007-Working Group I: The Physical Science 2007.

[2] IPCC. IPCC Special Report on Carbon Dioxide Capture and Storage. Prepared by Working Group III of the Intergovernmental Panel on Climate Change. Cambridge, United Kingdom and New York, NY, USA: Cambridge University Press; 2005.

[3] Li Z, Liu Y, Cai N. Understanding the enhancement effect of high-temperature steam on the carbonation reaction of CaO with CO_2. Fuel. 2014;127:88-93.

[4] Materić V, Symonds R, Lu D, Holt R, Manović V. Performance of Hydration Reactivated Ca Looping Sorbents in a Pilot-Scale, Oxy-fired Dual Fluid Bed Unit. Energy Fuels. 2014;28:5363-72.

[5] Itskos G, Grammelis P, Scala F, Pawlak-Kruczek H, Coppola A, Salatino P, et al. A comparative characterization study of Ca-looping natural sorbents. Appl Energy. 2013;108:373-82.

[6] Abanades JC, Murillo R, Fernandez JR, Grasa G, Martínez I. New CO_2 Capture Process for Hydrogen Production Combining Ca and Cu Chemical Loops. Environ Sci Technol. 2010;44:6901-4.

[7] Feng B. Sorbent regeneration. 2011;PCT/AU2011/000007, Australia

[8] Fernandez JR, Abanades JC, Grasa G. Modeling of sorption enhanced steam methane reforming—Part II: Simulation within a novel Ca/Cu chemical loop process for hydrogen production. Chem Eng Sci. 2012;84:12-20.

[9] Fernández JR, Abanades JC, Murillo R, Grasa G. Conceptual design of a hydrogen production process from natural gas with CO_2 capture using a Ca–Cu chemical loop. Int J Greenhouse Gas Control. 2012;6:126-41.

[10] Martínez I, Romano MC, Fernández JR, Chiesa P, Murillo R, Abanades JC. Process design of a hydrogen production plant from natural gas with CO_2 capture based on a novel Ca/Cu chemical loop. Appl Energy. 2014;114:192-208.

[11] Rahman RA, Mehrani P, Lu DY, Anthony EJ, Macchi A. Investigating the Use of CaO/CuO Sorbents for in Situ CO_2 Capture in a Biomass Gasifier. Energy Fuels. 2015.

[12] Qin C, Yin J, Liu W, An H, Feng B. Behavior of CaO/CuO Based Composite in a Combined Calcium and Copper Chemical Looping Process. Ind Eng Chem Res. 2012;51:12274-81.

[13] Qin C, Yin J, Luo C, An H, Liu W, Feng B. Enhancing the performance of CaO/CuO based composite for CO_2 capture in a combined Ca–Cu chemical looping process. Chem Eng J. 2013;228:75-86.

[14] Qin C, Feng B, Yin J, Ran J, Zhang L, Manovic V. Matching of kinetics of $CaCO_3$ decomposition and CuO reduction with CH_4 in Ca–Cu chemical looping. Chem Eng J. 2015;262:665-75.

[15] Ridha FN, Lu D, Macchi A, Hughes RW. Combined calcium looping and chemical looping combustion cycles with CaO–CuO pellets in a fixed bed reactor. Fuel. 2015;153:202-9.

[16] Kierzkoska A, Müller CR. Development of calcium-based, copper-functionalised CO_2 sorbents to

integrate chemical looping combustion into calcium looping. Energy Environ Sci. 2012;5:6061-5.

[17] Manovic V, Anthony EJ. Integration of calcium and chemical looping combustion using composite CaO/CuO-based materials. Environ Sci Technol. 2011;45:10750-6.

[18] Manovic V, Wu Y, He I, Anthony EJ. Core-in-Shell CaO/CuO-Based Composite for CO_2 Capture. Ind Eng Chem Res. 2011;50:12384-91.

[19] Georgakis C, Chang CW, Szekely J. A changing grain size model for gas—solid reactions. Chem Eng Sci. 1979;34:1072-5.

[20] García-Labiano F, Abad A, de Diego LF, Gayán P, Adánez J. Calcination of calcium-based sorbents at pressure in a broad range of CO_2 concentrations. Chem Eng Sci. 2002;57:2381-93.

[21] Mahuli SK, Agnihotr R, Jadhav R, Chauk S, Fan LS. Combined calcination, sintering and sulfation model for $CaCO_3$-SO_2 reaction. AICHE J. 1999;45:367-82.

[22] Yu YS, Liu WQ, An H, Yang FS, Wang GX, Feng B, et al. Modeling of the carbonation behavior of a calcium based sorbent for CO_2 capture. Int J Greenhouse Gas Control. 2012;10:510-9.

[23] Yin J, Kang X, Qin C, Feng B, Veeraragavan A, Saulov D. Modeling of $CaCO_3$ decomposition under CO_2/H_2O atmosphere in calcium looping processes. Fuel Process Technol. 2014;125:125-38.

[24] Sedghkerdar MH, Mahinpey N. A Modified Grain Model in Studying the CO_2 Capture Process with a Calcium-Based Sorbent: A Semianalytical Approach. Ind Eng Chem Res. 2015;54:869-77.

[25] Schlichting H, Gersten K. Boundary-Layer Theory. 8th ed. Berlin & New York: Springer; 2000.

[26] Juan Adánez, Francisco García-Labiano, Luis F. de Diego, Ainhoa Plata, Javier Celaya, Pilar Gayán, et al. Optimizing the Fuel Reactor for Chemical Looping Combustion. 17th International Conference on Fluidized Bed Combustion. Jacksonville, Florida, USA, 2003. p. 173-82.

[27] Fuller EN, Schettler PD, Giddings JC. New method for prediction of binary gas-phase diffusion coefficients. Ind. Eng. Chem. 1966;58:18-27.

[28] Ranz WE, Marshall WR. Evaporation from drops, Part I. Chem Eng Prog. 1952;48:141-6.

[29] Ranz WE, Marshall WR. Evaporation from drops, part II. Chem Eng Prog. 1952;48:173-80.

[30] Borgwardt RH. Calcination kinetics and surface area of dispersed limestone particles. AICHE J. 1985;31:103-11.

[31] García-Lario AL, Martínez I, Murillo R, Grasa G, Fernández JR, Abanades JC. Reduction Kinetics of a High Load Cu-based Pellet Suitable for Ca/Cu Chemical Loops. Ind Eng Chem Res. 2013;52:1481-90.

[32] Davidson ML, Harrison DP. Evaluation of the changing grain size model. Chem Eng Commun. 1984;25:213-28.

[33] García-Labiano F, de Diego LF, Adánez J, Abad A, Gayán P. Temperature variations in the oxygen carrier particles during their reduction and oxidation in a chemical-looping combustion system. Chem Eng Sci. 2005;60:851-62.

[34] Qin C, Yin J, Feng B, Ran J, Zhang L, Manovic V. Modelling of the calcination behaviour of a uniformly-distributed $CuO/CaCO_3$ particle in Ca–Cu chemical looping. Appl Energy. 2016;164:400-10.

Simulation of the calcination of a core-in-shell CuO/CaCO 3 particle for Ca–Cu chemical looping

Qin, Changlei

2016-05-12

Changlei Qin, Vasilije Manovic, Jingyu Ran, Bo Feng, Simulation of the calcination of a core-in-shell CuO/CaCO3 particle for Ca–Cu chemical looping, Fuel, Volume 181, 1 October 2016, Pages 522-530

http://dx.doi.org/10.1016/j.fuel.2016.05.035.